



PAPER

[View Article Online](#)
[View Journal](#)

Cite this: DOI: 10.1039/d5ta03943f

Eco-friendly non-volatile solid additives for high-efficiency sustainable organic photovoltaic cells†

Do Hui Kim,^a Heunjeong Lee,^a Dongchan Lee,^a Jiwoo Yeop,^b Jin Young Kim ^b and Shinuk Cho ^{*a}

As organic photovoltaics (OPVs) have become increasingly commercially viable in recent years, with power conversion efficiency (PCE) exceeding 20%, the importance of environmental sustainability has also grown significantly. While most eco-friendly OPV developments have focused on replacing solvents in the photoactive layer with benign alternatives, reliance on harmful additives for morphology modulation remains a major obstacle to achieving fully sustainable OPVs. This study presents the first example of a fully eco-friendly OPV, achieved by incorporating novel, non-volatile, eco-friendly solid additives, specifically, 4,4'-dihydroxybiphenyl (DBP), 4,4'-dimethylbiphenyl (DMBP), and 2,2'-dihydroxy-4-methoxybenzophenone (DM), in combination with the eco-friendly solvent *o*-xylene. Among them, DBP demonstrates the highest performance and long-term stability due to its superior miscibility and higher boiling point, achieving a PCE of 17.78%. Enhanced crystallinity and optimal phase separation morphology within the photoactive layer by DBP contribute to improvements in charge transfer, mobility, and device stability. This development marks a significant step toward the commercialization of sustainable OPVs, meeting the dual objectives of high efficiency and environmental compatibility.

Received 16th May 2025

Accepted 13th July 2025

DOI: 10.1039/d5ta03943f

rsc.li/materials-a

Introduction

Organic photovoltaics (OPVs) have emerged as one of the most promising candidates for eco-friendly energy solutions due to their inherent advantages, such as cost-effectiveness, mechanical flexibility, and lightweight properties.^{1,2} Recent advancements in OPVs, with power conversion efficiencies (PCEs) reaching up to 20%, have significantly enhanced their commercial viability.^{3–8} As this commercial potential grows, increasing attention is being directed toward the eco-friendliness of the materials employed in both the components and manufacturing processes of OPVs. Currently, research efforts are primarily focused on the eco-friendliness of the photoactive layer, the most critical component in determining the performance and sustainability of OPVs.

Conventional high-efficiency OPVs commonly employ halogenated solvents, such as chloroform (CF) and chlorobenzene (CB), in the fabrication of the photoactive layer. These solvents, however, pose significant environmental and health risks due to their toxicity and persistence in the environment.^{9–11} Consequently, considerable attention has been directed toward replacing halogenated solvents with non-halogenated,

environmentally friendly alternatives.^{12,13} However, one critical aspect that is often overlooked is the continued use of non-environmentally friendly additives in the process of forming the active layer to achieve optimal phase separation morphology.^{14–17} 1-Chloronaphthalene (CN) is a widely used halogenated solvent additive for optimizing the morphology of photoactive layers in Y-series non-fullerene acceptor (NFA)-based OPVs, achieving high PCEs.^{18–21} The OPV based on PM6:L8-BO, fabricated using the eco-friendly solvent *o*-xylene and the halogenated solvent additive CN, exhibited a PCE of 15.33% (Fig. S1†).

Recently, the use of solid additives, which are much more convenient to handle than solution-based additives, such as CN, 1,8-diiodooctane (DIO), and diphenyl ether (DPE), has become more widespread.^{22–25} Most eco-friendly solid additives reported to date have been volatile. While volatile solid additives offer the advantage of promoting crystallization of the photoactive layer during thin-film fabrication through evaporation, they present challenges in controlling volatility, which can hinder the reproducibility of performance. Furthermore, structural changes in the photoactive layer over time may compromise long-term stability. In contrast, non-volatile solid additives remain in the photoactive layer throughout both the fabrication process and device operation, helping to maintain stable phase separation within the layer. This facilitates the preservation of a stable photoactive layer structure over time, thereby improving the device's lifetime and performance stability. Additionally, higher reproducibility in the

^aDepartment of Semiconductor Physics and Engineering, University of Ulsan, Ulsan 44610, Republic of Korea. E-mail: sucho@ulsan.ac.kr

^bSchool of Energy and Chemical Engineering, Ulsan National Institute of Science and Technology (UNIST), Ulsan 44919, Republic of Korea

† Electronic supplementary information (ESI) available. See DOI: <https://doi.org/10.1039/d5ta03943f>

manufacturing process can be expected. Since both volatile and non-volatile solid additives have clear advantages and disadvantages, the choice between them should depend on the intended objective. However, for the commercialization of OPVs, where long lifespan and high stability are crucial, the importance of non-volatile additives is increasingly emphasized. However, non-volatile solid additives that are well compatible with eco-friendly solvents have not yet been reported.

In this study, we demonstrated the fully eco-friendly OPV by using newly developed, eco-friendly, non-volatile solid additives, such as 4,4'-dihydroxybiphenyl (DBP), 4,4'-dimethylbiphenyl (DMBP), and 2,2'-dihydroxy-4-methoxybenzophenone (DM), in combination with the eco-friendly solvent *o*-xylene. The eco-friendliness of the three selected additives was verified by checking their material safety data sheets (MSDSs). In this context, the term "eco-friendly" refers to halogen-free materials that were selected based on their relatively low toxicity, as indicated by the hazard symbols of the Globally Harmonized System (GHS). Nevertheless, additional factors such as environmental persistence, biodegradability, and life-cycle impact should also be considered to provide a more comprehensive assessment of eco-friendliness. These aspects remain important subjects for future research. All three additives contributed to improved performance when applied to PM6:L8-BO solar cells. Among them, DBP, with the highest boiling point, facilitated the formation of an optimal photoactive layer morphology, characterized by enhanced crystallinity due to its high miscibility with the donor and acceptor materials. This resulted in the development of a fully eco-friendly OPV with a power conversion efficiency (PCE) of 17.78%. The OPV also demonstrated high reproducibility and long-term stability when using DBP.

Results and discussion

For the photoactive materials, PM6 and L8-BO were utilized. Fig. 1a shows the chemical structures of the donor PM6 and the acceptor L8-BO. Although the PCE of PM6:L8-BO solar cells varies depending on the types of electron transport layer (ETL) and hole transport layer (HTL), as well as specific fabrication conditions, it has been reported to range between approximately 16.0–18.0%. In our laboratory, we fabricated cells using PDINN ETL and Br-2EPSe HTL,²⁶ along with the commonly employed CF solvent and CN additive. Under these conditions, the PCE reached approximately 16.74% (Fig. S1†). However, when *o*-xylene was used as a solvent instead of CF, the PCE slightly decreased to 15.33% (Fig. S1†). This is a commonly observed phenomenon, as *o*-xylene is known to induce aggregation of the non-fullerene acceptor (NFA) in the photoactive layer.^{27–29} Similar aggregation issues in photoactive materials have often been addressed using additives in the past. Based on this idea, to mitigate the performance degradation caused by non-halogenated solvents, we decided to introduce non-volatile solid additives. Furthermore, we ensured that the additives were environmentally friendly. We introduced and compared the performance of three such eco-friendly, non-volatile additives –

DBP, DMBP, and DM – as shown in Fig. 1b. For reference, the boiling points (Bp) of DBP, DMBP, and DM are 355 °C, 295 °C, and 170 °C, respectively. And the melting points (Mp) of DBP, DMBP, and DM are 282 °C, 120 °C, and 75 °C, respectively.

Initially, we investigated whether three eco-friendly non-volatile additives influence the band structure through chemical interactions with photoactive materials by conducting UV-vis measurements on PM6 and L8-BO films containing the additives. In the case of PM6 (Fig. 1c), the position of the maximum absorption peak remained the same, regardless of the presence or type of additives, and the onset edge, which provides information about the band gap, was also observed to be identical in all cases. This suggests that there are no significant chemical interactions between the added additives and PM6 that could affect the energy levels. However, they appear to clearly influence the physical packing structure. Specifically, the intensity ratio of the 0–0 peak to the 0–1 peak in the PM6 film with DBP increased, indicating that DBP promotes more ordered molecular stacking in PM6.^{30,31} In the case of L8-BO, similar to PM6, minimal chemical interaction is observed. However, it appears to be more significantly affected by molecular packing. As shown in Fig. 1d, the normalized absorption spectra of L8-BO films with various additives reveal that films containing eco-friendly solid additives exhibit slight red shifts compared to the film without additives. Additionally,

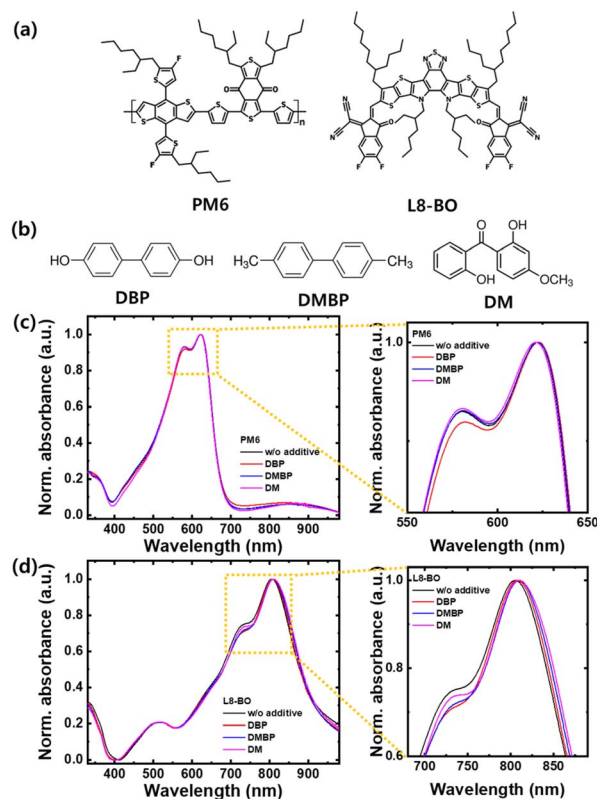


Fig. 1 Chemical structures of (a) the polymer donor PM6 and the non-fullerene acceptor L8-BO, and (b) the eco-friendly solid additives DBP, DMBP, and DM. Normalized absorption spectra of (c) PM6 and (d) L8-BO films with and without DBP, DMBP, and DM.

the ratios of the 0–0 peak intensity to the 0–1 peak intensity were altered. Among these films, the one with DBP exhibited the most ordered molecular stacking.

Fig. S2 and S3† show the 2D GIWAXS scattering patterns of PM6 and L8-BO films with different additives, respectively. As previously discussed, the π – π stacking distance of PM6 remains largely unchanged regardless of the additive. In contrast, L8-BO exhibits a notable variation in π – π stacking distance depending on the additive, with the eco-friendly solid additive promoting more favorable molecular stacking. Notably, DBP leads to the most enhanced molecular packing of L8-BO.

To investigate the intermolecular interactions between the additives (DBP, DMBP, and DM) and the active materials, FTIR measurements were carried out on PM6 and L8-BO films with and without each additive.^{32–35} As shown in Fig. S4,† the PM6 films exhibited a characteristic carbonyl peak at 1651.4 cm^{-1} , with no significant changes upon the addition of the additives. In contrast, the L8-BO films exhibited noticeable peak shifts upon the addition of the additives. These shifts occurred in the characteristic peaks corresponding to alkyl chain vibrations ($\sim 1423\text{ cm}^{-1}$), C=C stretching ($\sim 1532\text{ cm}^{-1}$), and cyano group vibrations ($\sim 2215\text{ cm}^{-1}$). The peak shift in alkyl chain vibrations was most pronounced in L8-BO with DBP compared to L8-BO with DMBP or DM, indicating stronger intermolecular interactions between L8-BO and DBP. These FTIR results suggest that DBP, DMBP, and DM enhance intermolecular interactions more effectively with L8-BO than with PM6, with DBP showing the most significant effect.

This tendency was further corroborated by atomic force microscopy (AFM) measurements of neat PM6 and L8-BO films with additives. Fig. 2a and b present the AFM topographic images of PM6 and L8-BO films, both with and without eco-

friendly solid additives. The corresponding phase images are shown in Fig. S5.† The morphology of pristine PM6 films remained largely similar with or without additives, except in the case of DBP, which resulted in a more uniform morphology. In contrast, the AFM topographic images of L8-BO films show distinct differences depending on the additive used, as displayed in Fig. 2b. The L8-BO film with DM, an additive with the lowest boiling point and melting point, exhibited a more aggregated morphology compared to the L8-BO film with DBP, which has the highest boiling point and melting point. This suggests that the morphology of L8-BO is sensitive to the volatility of the additives, with additives that volatilize more rapidly impeding the formation of an optimal morphology. Therefore, selecting the appropriate additive is critical for achieving the desired morphology in the photoactive layer.

Fig. 2c illustrates the blend morphology of PM6:L8-BO films with and without eco-friendly solid additives. The blend film without additives formed a non-uniform morphology and had a root-mean-square (RMS) roughness value of 2.474 nm , indicating relatively poor miscibility between the donor and acceptor. In contrast, the blend films containing eco-friendly solid additives exhibited a smoother and more uniform surface. The films with DBP and DMBP, which have higher boiling points than DM, formed a distinct fibrillar structure compared to the blend film with DM. Specifically, the PM6:L8-BO blend film with DBP had an RMS roughness value of 1.340 nm , resulting in a smoother and more uniform morphology, which is attributed to the improved miscibility between PM6 and L8-BO due to the introduction of DBP.

The miscibility between the donor and acceptor is critical for forming the desired interpenetrating nanoscale morphology in the photoactive layer of a bulk-heterojunction (BHJ) structure. To evaluate the miscibility between PM6 and L8-BO in the presence of different additives, contact angle measurements were performed. The Flory–Huggins interaction parameters (χ) were calculated using the equation $\chi_{1,2} = K(\sqrt{\gamma_1} - \sqrt{\gamma_2})^2$, where γ represents surface energy and K is a proportionality constant.^{30,36} Fig. S6† shows the contact angle images of PM6 and L8-BO thin films with and without additives, with detailed data provided in Table S4.† The calculated χ values between PM6 and L8-BO were $0.0426K$ without additives, $0.0235K$ with DBP, $0.0293K$ with DMBP, and $0.0410K$ with DM. A lower χ value indicates better miscibility between PM6 and L8-BO. Overall, the miscibility between the materials improved with the use of eco-friendly additives, with DBP showing the most significant enhancement.

As shown in Fig. S7,† the fibril widths of PM6:L8-BO films with and without eco-friendly solid additives were determined from the full width at half maximum (FWHM) of the peaks in the line-cut profiles of the AFM phase images.^{37,38} The calculated average values were 30.84 nm , 19.82 nm , 24.43 nm , and 25.37 nm for PM6:L8-BO films without additives and with DBP, DMBP, and DM, respectively. The blend films containing eco-friendly solid additives exhibited relatively smaller fibril widths compared to the film without additives. This is attributed to the enhanced miscibility between the donor and

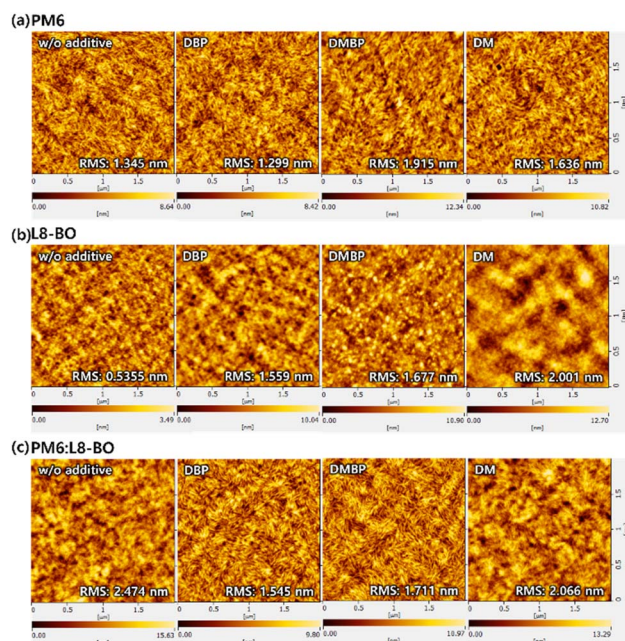


Fig. 2 AFM topographic images of (a) PM6, (b) L8-BO, and (c) PM6:L8-BO blend films without additives, and with DBP, DMBP, and DM.

acceptor induced by the additives. In particular, DBP, which promoted the highest miscibility, facilitated the formation of the finest and most uniformly distributed fibrils.

GIWAXS measurements were conducted to investigate the molecular packing and crystallinity of the photoactive layer. The 2D GIWAXS patterns and corresponding line-cut profiles of the PM6:L8-BO blend films, both with and without eco-friendly

solid additives, are shown in Fig. 3 and Table S5,[†] respectively. All PM6:L8-BO blend films exhibited a pronounced π - π stacking peak in the out-of-plane (OOP) direction, indicating a preference for face-on orientation. The PM6:L8-BO blend films with eco-friendly solid additives showed relatively smaller d -spacing values of 3.564 \AA^{-1} for DBP, 3.572 \AA^{-1} for DMBP, and 3.576 \AA^{-1} for DM, compared to 3.607 \AA^{-1} for the blend film without additives. Furthermore, the corresponding coherence lengths (L_c) in the OOP direction increased from 25.24 \AA in the film without additives to 27.72 \AA for DBP, 27.32 \AA for DMBP, and 26.93 \AA for DM. Notably, the use of DBP as an eco-friendly solid additive significantly enhanced the intermolecular packing and crystallinity of the PM6:L8-BO blend film, which is promising for improving charge transfer properties and device performance.

Fourier-transform infrared spectroscopy (FTIR) measurements were conducted to confirm the volatility of the additives in the photoactive layer, as shown in Fig. 4a-c.^{39,40} DBP exhibited a characteristic FTIR absorption peak at 1627.03 cm^{-1} , which was also present in the FTIR absorption spectra of the PM6:L8-BO blend film with DBP. Notably, this characteristic peak did not disappear even after thermal treatment (130°C for 10 min), indicating that DBP, with its high boiling point, was not volatilized and remained within the photoactive layer. In contrast, DMBP and DM, which have lower boiling points, showed different behavior. DMBP exhibited a characteristic FTIR absorption peak at 803.77 cm^{-1} , visible in the PM6:L8-BO blend film before thermal treatment, but it disappeared after thermal treatment. Similarly, in the PM6:L8-BO blend film with DM before thermal treatment, characteristic peaks of DM were observed at 1028.62 , 968.99 , 925.26 , and 760.05 cm^{-1} .

These peaks vanished after thermal treatment, indicating that DM was volatilized. Although the criteria for determining

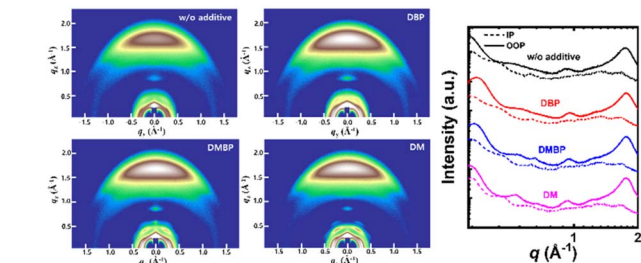


Fig. 3 2D GIWAXS scattering patterns and corresponding line-cut profiles of PM6:L8-BO blend films without additives, and with DBP, DMBP, and DM.

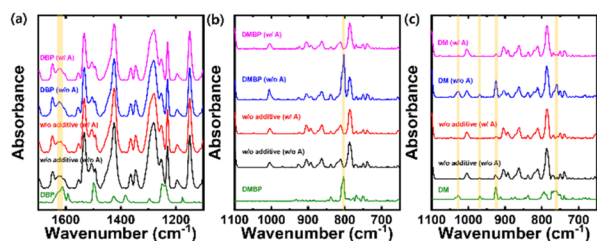


Fig. 4 FTIR spectra of PM6:L8-BO blend films with (a) DBP, (b) DMBP, and (c) DM, with and without annealing treatment.

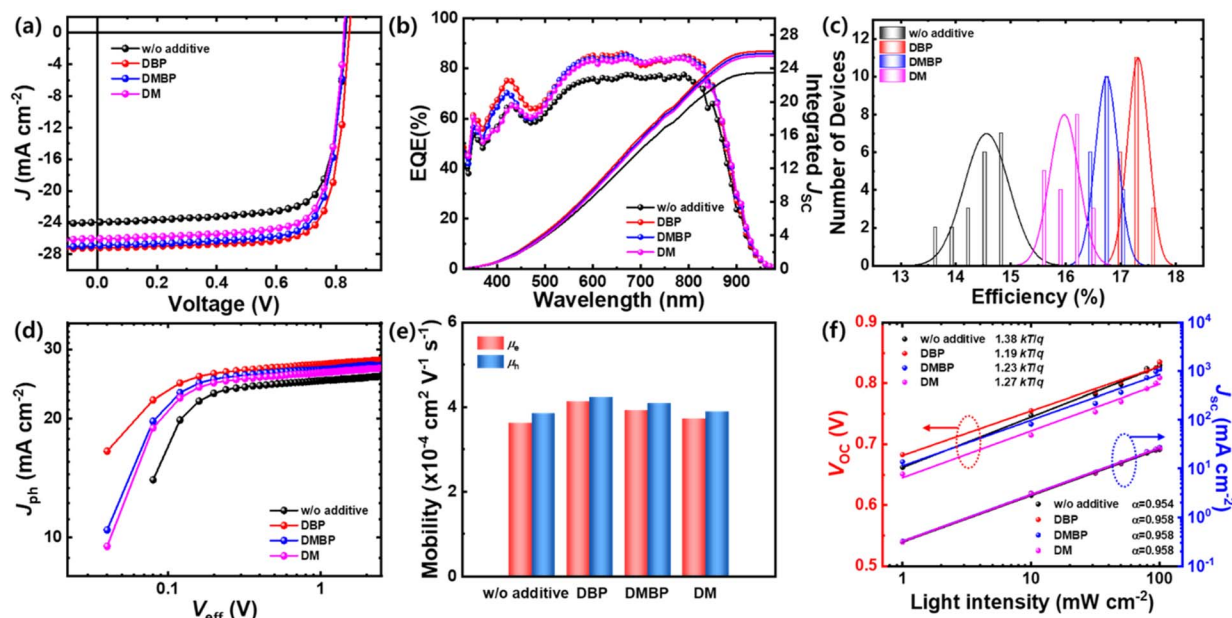


Fig. 5 (a) J - V characteristic curves, (b) EQE spectra, (c) statistical histograms of device efficiency, (d) J_{ph} - V_{eff} curves, (e) electron and hole mobilities, and (f) light dependence of J_{sc} and V_{oc} in OPVs based on PM6:L8-BO without and with DBP, DMBP, and DM.

the volatility or non-volatility of additives at a specific reference point have not yet been clearly established, if this assessment is made during the spin-coating process that forms the film, all three eco-friendly additives could be classified as non-volatile. However, if the evaluation point is extended to include the operational phase after the complete fabrication of the device, DBP can be clearly categorized as a non-volatile additive, whereas DMBP and DM would be classified as volatile. In the case of DM, which has a relatively low Bp of 170 °C, its evaporation during annealing at 130 °C is understandable. However, it is somewhat surprising that DMBP, despite having a Bp of 295 °C, mostly evaporated after annealing at 130 °C for 10 minutes. This suggests that the volatility or non-volatility of an additive should be determined by considering various factors, such as its boiling point and melting point. In addition, it should be comprehensively evaluated based on whether the additive remains under actual processing conditions, including both immediately after spin-coating and after post-annealing.

To investigate the effects of eco-friendly solid additives on device performance, an OPV with a conventional structure of ITO/Br-2EPSe/PM6:L8-BO/PDINN/Ag was fabricated. The current density–voltage (J – V) curves and detailed parameters of the optimized OPV are shown in Fig. 5a and Table 1. The optimal amounts of DBP, DMBP, and DM were explored, as shown in Fig. S10–S12 and Tables S6–S8.† The device without additives exhibited a PCE of 15.01%, with a short-circuit current density (J_{SC}) of 24.00 mA cm^{−2}, an open-circuit voltage (V_{OC}) of 0.832 V, and a fill factor (FF) of 75.16%. All OPVs with eco-friendly solid additives demonstrated higher performance compared to both the OPV with CN (Fig. S1 and Table S1†) and the one without additives. Among them, DBP, with its non-volatile properties, achieved the highest PCE of 17.78%, with a J_{SC} of 27.18 mA cm^{−2}, a V_{OC} of 0.845 V, and a FF of 77.43%. The PCE of devices with DMBP and DM also increased to 17.13% and 16.46%, respectively. However, unlike DBP, V_{OC} did not improve in these devices, and in the case of DM, which has a low boiling point, V_{OC} was reduced. The adoption of eco-friendly solid additives notably enhanced the J_{SC} and FF of the devices, likely due to improvements in the morphology and crystallinity of the photoactive layer. Fig. 5b shows the external quantum efficiency (EQE) spectra of the devices with and without additives. The devices with DBP, DMBP, and DM exhibited significantly enhanced photogenerated current responses compared to the device without additives, consistent with the observed J_{SC} values. Fig. 5c presents the statistical histograms of OPV efficiency with and without eco-friendly solid additives. The average efficiency of devices with eco-friendly

additives was higher than those without additives, and these additives had a similar effect when applied to PM6:BTP-eC9 OPVs (Fig. S13–S15 and Tables S9–S11†).

To investigate the process of exciton dissociation and charge extraction, the photocurrent density–effective voltage (J_{ph} – V_{eff}) characteristics were measured, as shown in Fig. 5d. The maximum exciton generation rate (G_{max}) of the devices was calculated using the equation $G_{max} = J_{sat}/qL$, where J_{sat} is the saturation photocurrent density, q is the elementary charge, and L is the thickness of the photoactive layer.^{41,42} The calculated G_{max} values were $1.61 \times 10^{28} \text{ m}^{-3} \text{ s}^{-1}$, $1.75 \times 10^{28} \text{ m}^{-3} \text{ s}^{-1}$, $1.70 \times 10^{28} \text{ m}^{-3} \text{ s}^{-1}$, and $1.67 \times 10^{28} \text{ m}^{-3} \text{ s}^{-1}$ for the devices without additives, and with DBP, DMBP, and DM, respectively. The introduction of eco-friendly solid additives increased the G_{max} values, with DBP yielding the highest value. This increase correlates with the enhanced light absorption of the photoactive layers containing DBP. The exciton dissociation efficiency (P_{diss}) and charge collection efficiency (P_{coll}) were determined from J_{ph}/J_{sat} under short-circuit conditions and maximum power output conditions, respectively.^{43–45} Devices with eco-friendly solid additives exhibited higher P_{diss} and P_{coll} values compared to the device without additives. The estimated P_{diss} values were similar, at approximately 97.0% for all devices with additives, while the device with DBP achieved the highest P_{coll} of 89.6%. This indicates that the enhanced J_{SC} and FF of the device with DBP are due to its improved exciton dissociation and charge collection capabilities.

The carrier mobility of the device upon the introduction of eco-friendly solid additives was investigated using the space charge limited current (SCLC) method. Fig. 5e and Table S12† illustrate that the electron mobilities (μ_e) for the devices with DBP, DMBP, and DM increased from $3.61 \times 10^{-4} \text{ cm}^2 \text{ V}^{-1} \text{ s}^{-1}$ to $4.13 \times 10^{-4} \text{ cm}^2 \text{ V}^{-1} \text{ s}^{-1}$, $3.91 \times 10^{-4} \text{ cm}^2 \text{ V}^{-1} \text{ s}^{-1}$, and $3.72 \times 10^{-4} \text{ cm}^2 \text{ V}^{-1} \text{ s}^{-1}$, respectively. Additionally, the devices with DBP, DMBP, and DM exhibited higher hole mobilities (μ_h) of $4.22 \times 10^{-4} \text{ cm}^2 \text{ V}^{-1} \text{ s}^{-1}$, $4.08 \times 10^{-4} \text{ cm}^2 \text{ V}^{-1} \text{ s}^{-1}$, and $3.89 \times 10^{-4} \text{ cm}^2 \text{ V}^{-1} \text{ s}^{-1}$ compared to the device without additive. This improvement in carrier mobility is inferred to be due to the enhanced crystallinity of the photoactive layers facilitated by the eco-friendly solid additives.⁴⁶ Notably, DBP not only demonstrated the highest electron and hole mobilities but also achieved the most balanced μ_e/μ_h ratio of 0.978, contributing to a high FF of the device.

The transient photocurrent (TPC) and transient photovoltage (TPV) measurements were conducted to investigate the effect of additives on the charge extraction and recombination behavior of the device, as shown in Fig. S17 and Table S13.† The charge

Table 1 Detailed photovoltaic parameters of devices based on PM6:L8-BO without and with DBP, DMBP, and DM. The average values were calculated from 20 devices

Additive	J_{SC} (mA cm ^{−2})	V_{OC} (V)	FF	PCE (%)
Without additive	24.00 (23.63 ± 0.355)	0.832 (0.828 ± 0.006)	75.16 (74.32 ± 1.275)	15.01 (14.55 ± 0.399)
DBP	27.18 (26.86 ± 0.458)	0.845 (0.843 ± 0.009)	77.43 (76.43 ± 0.478)	17.78 (17.31 ± 0.188)
DMBP	26.91 (26.41 ± 0.351)	0.830 (0.826 ± 0.004)	76.74 (76.69 ± 0.497)	17.13 (16.74 ± 0.200)
DM	26.07 (26.00 ± 0.292)	0.826 (0.814 ± 0.007)	76.38 (75.43 ± 0.816)	16.46 (15.97 ± 0.257)

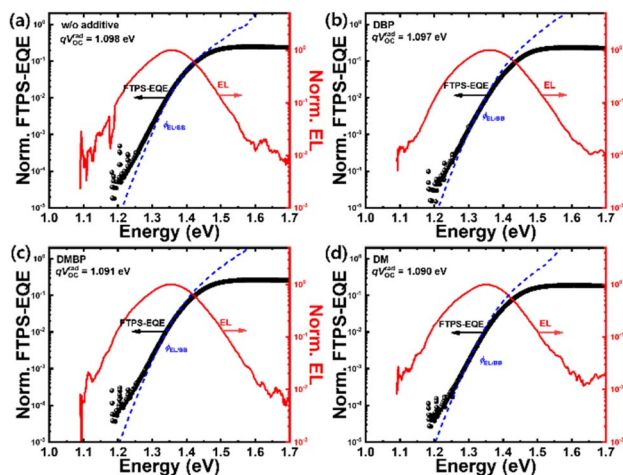


Fig. 6 FTPS-EQE and EL spectra of OPVs based on PM6:L8-BO (a) without additives and with (b) DBP, (c) DMBP, and (d) DM.

extraction times (τ_t) for the devices without additive, and with DBP, DMBP, and DM were 0.405 μ s, 0.293 μ s, 0.322 μ s, and 0.314 μ s, respectively. Overall, the devices with eco-friendly solid additives exhibited faster charge extraction times, with the device containing DBP demonstrating the most effective charge extraction capability. Furthermore, the device with DBP showed the longest charge carrier lifetime (τ_r) of 1.76 μ s, compared to 1.13 μ s, 1.63 μ s, and 1.65 μ s for the device without additive, and those with DMBP and DM, respectively. This suggests that the faster charge extraction and inhibited charge recombination observed in the device with DBP can be attributed to improved molecular stacking.

To verify the charge recombination behaviors, the dependence of J_{SC} and V_{OC} on light intensity (P_{light}) was measured. The relationship between J_{SC} and P_{light} is expressed by the power law equation $J_{SC} \propto (P_{light})^\alpha$. The dependence of V_{OC} on P_{light} follows the equation $V_{OC} \propto (nkT/q)\ln(P_{light})$, where k is the Boltzmann constant, T is the temperature in Kelvin, and q is the elementary charge.^{47,48} As shown in Fig. 5f, the extracted α values for all devices, both with and without eco-friendly solid additives, were nearly identical. In contrast, the n values exhibited distinct behavior. The extracted n value for the device without additive was $1.38(kT/q)$, while the values for the devices with DBP, DMBP, and DM were $1.19(kT/q)$, $1.23(kT/q)$, and $1.27(kT/q)$, respectively. The device with DBP exhibited the lowest n value, indicating that the DBP eco-friendly solid additive most effectively suppressed trap-assisted recombination in the device.

The device with DBP exhibited a higher V_{OC} compared to the devices without additive and those with DMBP and DM. To

investigate this further, energy loss analysis was conducted through Fourier-transform photocurrent spectroscopy external quantum efficiency (FTPS-EQE) and electroluminescence (EL) spectra measurements, as shown in Fig. 6 and Table 2. The total energy loss (ΔE_{loss}) values for the devices without additive, and with DMBP and DM were nearly identical, calculated at 0.574 eV, 0.572 eV, and 0.575 eV, respectively. In contrast, the device with DBP exhibited the lowest energy loss of 0.559 eV. Although the devices with DMBP and DM showed a reduction in ΔE_3 due to improved crystallinity of the photoactive layer compared to the device without additives, they were unable to overcome the radiative recombination loss (ΔE_2) due to their volatile characteristics, resulting in ΔE_{loss} values similar to those of the device without additive.⁴⁹ Conversely, the non-volatile eco-friendly solid additive DBP effectively minimized ΔE_2 loss, while enhanced molecular stacking and crystallinity significantly reduced the non-radiative recombination loss (ΔE_3), resulting in a higher V_{OC} .

Fig. 7 shows the long-term storage stability of the devices with DBP, DMBP, and DM additives. The devices were stored in an N_2 atmosphere under dark conditions without encapsulation. All three additives exhibited slightly improved stability compared to the representative solvent-based volatile additive CN. Due to the significant performance degradation when using CN as an additive in *o*-xylene solvent, devices fabricated with CN were used for comparison to evaluate device stability under optimal performance conditions. Over the initial 300 hours, the device with DM showed a more rapid decrease in efficiency compared to the devices with DBP and DMBP. After 600 hours, the device with DBP maintained approximately 82% of its initial efficiency up to 1000 hours, whereas the devices with DMBP and DM relatively steeper decline in efficiency up to 1000 hours, dropping below 80%. To further investigate the thermal and photo-stability of the devices, thermal stability was evaluated by storing the devices under dark conditions in a nitrogen atmosphere at 70 $^{\circ}C$. Photo-stability was assessed by irradiating the devices with a 100 mW cm^{-2} white LED under ambient air. As

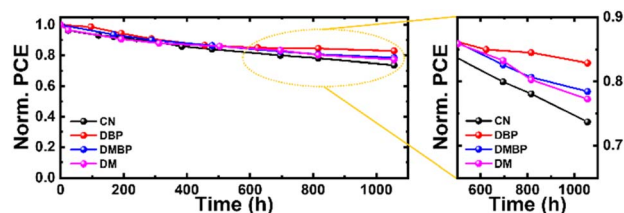


Fig. 7 Long-term storage stability of OPVs based on PM6:L8-BO with CN, DBP, DMBP, and DM.

Table 2 Detailed E_{loss} parameters of devices based on PM6:L8-BO without and with DBP, DMBP, and DM. The units of all the parameters are (eV)

Additive	E_g	qV_{OC}^{SC}	qV_{OC}^{rad}	qV_{OC}	ΔE_1	ΔE_2	ΔE_3 (EL/BB)	ΔE_3 (EQE _{EL})	ΔE_{loss}
Without additive	1.406	1.125	1.098	0.832	0.281	0.027	0.266	0.279	0.574
DBP	1.404	1.124	1.097	0.845	0.280	0.027	0.252	0.258	0.559
DMBP	1.402	1.122	1.091	0.830	0.280	0.031	0.261	0.267	0.572
DM	1.401	1.121	1.090	0.826	0.280	0.031	0.264	0.277	0.575

shown in Fig. S19,† in both thermal and photo-stability tests, the device with CN exhibited rapid degradation within 48 hours. In contrast, the devices with DBP, DMBP, and DM solid additives showed overall higher stability compared to the device with CN. Among them, the device with DBP demonstrated the highest stability, retaining over 73% of its initial efficiency after 200 hours under both thermal and photo-stability conditions. These results suggest that non-volatile DBP, with the highest boiling point, acted as a stabilizer for phase separation within the active layer over the long term, enhancing morphological stability and contributing to the device's long-term stability.

Conclusions

This study successfully demonstrated a fully eco-friendly OPV by incorporating non-volatile, eco-friendly solid additives, specifically DBP, DMBP, and DM, alongside the eco-friendly solvent *o*-xylene. DBP, with its high boiling point and enhanced miscibility with photoactive materials, significantly improved device performance and stability, achieving a PCE of 17.78%. Comparative analyses of the additives showed that DBP promoted an ordered molecular stacking and an optimal morphology, which enhanced charge transfer and reduced recombination. Moreover, the non-volatile nature of DBP contributed to long-term device stability, maintaining 82% of its initial efficiency after 1000 hours of storage. These findings highlight the potential of non-volatile, eco-friendly solid additives in advancing sustainable OPVs that balance high efficiency with environmental responsibility.

Data availability

The data supporting this article have been included as part of the ESI.†

Conflicts of interest

There are no conflicts to declare.

Acknowledgements

This work was supported by the Research Fund of University of Ulsan (2025-0327).

References

- 1 C. Liu, C. Xiao, C. Xie and W. Li, *Nano Energy*, 2021, **89**, 106399.
- 2 L. Sun, W. Zeng, C. Xie, L. Hu, X. Dong, F. Qin, W. Wang, T. Liu, X. Jiang, Y. Jiang and Y. Zhou, *Adv. Mater.*, 2020, **32**, 1907840.
- 3 T. Xu, G. Ran, Z. Luo, Z. Chen, J. Lv, G. Zhang, H. Hu, W. Zhang and C. Yang, *Small*, 2024, **20**, 2405476.
- 4 P. Wang, F. Bi, H. Jiang, X. Wang, C. Cui, Y. Li and X. Bao, *Adv. Funct. Mater.*, 2024, **35**, 2411862.
- 5 H. Mao, J. Zhang, X. Cen, J. Zhang, L. Wen, J. Xue, D. Luo, L. Zhang, Z. Qin, W. Ma, L. Tan and Y. Chen, *Energy Environ. Sci.*, 2024, **17**, 6799–6810.
- 6 K. Liu, Y. Jiang, G. Ran, F. Liu, W. Zhang and X. Zhu, *Joule*, 2024, **8**, 835.
- 7 H. Liang, K. Ma, S. Ding, W. Zhao, X. Si, X. Cao, Z. Yao, T. Duan, G. Long, C. Li, X. Wan and Y. Chen, *Adv. Energy Mater.*, 2024, **14**, 2402370.
- 8 Q. Li, X. Liao, Z. Yang, S. Zhang, R. Chen, L.-M. Wang, X. Zhan, S. Yuan, T. Jia, Y. Meng, Y.-P. Cai, H. Zhu, Y. Fu, G. Cai and S. Liu, *Nano Energy*, 2024, **129**, 110067.
- 9 C. Liu, J. Liu, X. Duan and Y. Sun, *Adv. Sci.*, 2023, **10**, 2303842.
- 10 H. Li, S. Liu, X. Wu, S. Yao, X. Hu and Y. Chen, *Energy Environ. Sci.*, 2023, **16**, 76–88.
- 11 S. Lee, D. Jeong, C. Kim, C. Lee, H. Kang, H. Y. Woo and B. J. Kim, *ACS Nano*, 2020, **14**, 14493–14527.
- 12 R. Ma, H. Li, T. A. D. Peña, H. Wang, C. Yan, P. Cheng, J. Wu and G. Li, *Natl. Sci. Rev.*, 2024, **11**, nwae384.
- 13 L. Chen, J. Yi, R. Ma, T. A. D. Peña, Y. Luo, Y. Wang, Y. Wu, Z. Zhang, H. Hu, M. Li, J. Wu, G. Zhang, H. Yan and G. Li, *Mater. Sci. Eng., R*, 2024, **159**, 100794.
- 14 J. Zhang, Q. Zhou, J. Xie, J. Zhao, J. Yu, K. Zhang, T. Jia, F. Huang and Y. Cao, *Adv. Funct. Mater.*, 2024, **34**, 2313722.
- 15 T. Huang, S. Geng, D. Wang, Y. Zhang, N. Weng, X. Li, Q. Liao, Z. Zhang, J. Lu and J. Zhang, *Adv. Funct. Mater.*, 2024, **34**, 2315825.
- 16 Y. J. Su, H. Nie, C. F. Chang, S. C. Huang, Y. H. Huang, T. W. Chen, K. K. Hsu, T. Y. Lee, H. M. Shih, C. W. Ko, J. T. Chen and C. S. Hsu, *ACS Appl. Mater. Interfaces*, 2021, **13**, 59043–59050.
- 17 S. Bao, H. Yang, H. Fan, J. Zhang, Z. Wei, C. Cui and Y. Li, *Adv. Mater.*, 2021, **33**, 2105301.
- 18 J. Zhu, Z. Qin, A. Lan, S. Jiang, J. Mou, Y. Ren, H. Do, Z.-K. Chen and F. Chen, *Small*, 2024, **20**, 2305529.
- 19 M. Zhang, B. Chang, R. Zhang, S. Li, X. Liu, L. Zeng, Q. Chen, L. Wang, L. Yang, H. Wang, J. Liu, F. Gao and Z.-G. Zhang, *Adv. Mater.*, 2024, **36**, 2308606.
- 20 T. Lin, Y. Hai, Y. Luo, L. Feng, T. Jia, J. Wu, R. Ma, T. A. Dela Peña, Y. Li, Z. Xing, M. Li, M. Wang, B. Xiao, K. S. Wong, S. Liu and G. Li, *Adv. Mater.*, 2024, **36**, 2312311.
- 21 X. Si, Y. Huang, W. Shi, R. Wang, K. Ma, Y. Zhang, S. Wu, Z. Yao, C. Li, X. Wan and Y. Chen, *Adv. Funct. Mater.*, 2023, **33**, 2306471.
- 22 S. Shen, Y. Mi, Y. Ouyang, Y. Lin, J. Deng, W. Zhang, J. Zhang, Z. Ma, C. Zhang, J. Song and Z. Bo, *Angew. Chem.*, 2023, **135**, e202316495.
- 23 W. Zhang, K. Zhao, N. Zhang, Q. Dong, S. Shen, H. Lu, B. Hu, F. Zhao, S. Yuan, G. Lu, Y. Chen, Z. Ma, Z. Bo and J. Song, *Adv. Funct. Mater.*, 2025, **35**, 2423242.
- 24 S. Shen, H. Lu, R. Zhu, W. Zhang, F. Zhao, C. Zhu, W. Liu, K. Zhao, J. Deng, W. Ma, Z. Ma, Y. Chen, Z. Kan, J. Song and Z. Bo, *CCS Chem.*, 2025, DOI: [10.31635/ccschem.025.202505659](https://doi.org/10.31635/ccschem.025.202505659).
- 25 S. Shen, W. Liu, H. Lu, W. Zhang, F. Zhao, B. Hu, Z. Suo, K. Zhao, J. Deng, Y. Mi, S. Yuan, Z. Ma, Y. Chen, Y. Liu,

- Z. Ma, G. Lu, X. Wan, Z. Bo and J. Song, *Adv. Funct. Mater.*, 2025, DOI: [10.1002/adfm.202507288](https://doi.org/10.1002/adfm.202507288).
- 26 A. Ullah, K. H. Park, Y. Lee, S. Park, A. B. Faheem, H. D. Nguyen, Y. Siddique, K.-K. Lee, Y. Jo, C.-H. Han, S. Ahn, I. Jeong, S. Cho, B. Kim, Y. S. Park and S. Hong, *Adv. Funct. Mater.*, 2022, **32**, 2208793.
 - 27 B. Kim, Y.-S. Lee, D. Um, W. Jeong, S. Lee, K. Kim, G. Nam, H. Hwang, S. Kim, T. Kim, K. Lee, H. Kang and B. Kim, *Adv. Funct. Mater.*, 2024, **34**, 2407403.
 - 28 Z. Abbas, S. U. Ryu, M. Haris, C. E. Song, H. K. Lee, S. K. Lee, W. S. Shin, T. Park and J.-C. Lee, *Nano Energy*, 2022, **101**, 107574.
 - 29 S. Dong, T. Jia, K. Zhang, J. Jing and F. Huang, *Joule*, 2020, **4**, 2004–2016.
 - 30 J. Xie, J. Deng, Y. Pei, S. Y. Jeong, B. Huang, D. Zhou, H. Y. Woo, J. Xu, F. Wu and L. Chen, *Adv. Funct. Mater.*, 2024, **34**, 2402281.
 - 31 J. Song, C. Li, H. Ma, B. Han, Q. Wang, X. Wang, D. Wei, L. Bu, R. Yang, H. Yan and Y. Sun, *Adv. Mater.*, 2024, **34**, 2406922.
 - 32 N. Wei, H. Lu, Y. Wei, Y. Guo, H. Song, J. Chen, Z. Yang, Y. Cheng, Z. Bian, W. Zhang, Q. Chen, Y. Liu, W. Zhao, X. Xu and Z. Bo, *Energy Environ. Sci.*, 2025, **18**, 2298.
 - 33 X. Li, Y. Wu, H. Yang, H. Fan, K. Hu, C. Cui and Y. Li, *Adv. Funct. Mater.*, 2025, DOI: [10.1002/adfm.202503986](https://doi.org/10.1002/adfm.202503986).
 - 34 Z. Zhang, Q. Chen, C. Zhang, W. L. Tan, G. Zhang, Z. Bu, C. Xiao, X. Shen, Z. Tang, C. R. McNeill and W. Li, *Adv. Funct. Mater.*, 2024, **34**, 2401823.
 - 35 F. Wang, J. Yu, S. Wang, M. Zhu, M. Xiao, W. Zhu and H. Tan, *Chem. Eng. J.*, 2024, **485**, 150081.
 - 36 X. Song, K. Zhang, R. Guo, K. Sun, Z. Zhou, S. Huang, L. Huber, M. Reus, J. Zhou, M. Schwartzkopf, S. V. Roth, W. Liu, Y. Liu, W. Zhu and P. Muller-Buschbaum, *Adv. Mater.*, 2022, **34**, 2200907.
 - 37 Y. Cai, Q. Li, G. Lu, H. S. Ryu, Y. Li, H. Jin, Z. Chen, Z. Tang, G. Lu, X. Hao, H. Y. Woo, C. Zhang and Y. Sun, *Nat. Commun.*, 2022, **13**, 2369.
 - 38 G. Ding, T. Chen, M. Wang, X. Xia, C. He, X. Zheng, Y. Li, D. Zhou, X. Lu, L. Zuo, Z. Xu and H. Chen, *Nano-Micro Lett.*, 2023, **15**, 92.
 - 39 J. Xu, C. Xiao, Z. Zhang, J. Zhang, B. Wang, C. R. McNeill and W. Li, *Small*, 2024, **20**, 2405573.
 - 40 L. Kong, X. Wang, M. Li, Z. Zhang, M. Chen, L. Zhang, L. Ying, D. Ma and J. Chen, *Adv. Energy Mater.*, 2024, **14**, 2402517.
 - 41 X. Yuan, H. Chen, S. Kim, Y. Chen, Y. Zhang, M. Yang, Z. Chen, C. Yang, H. Wu, X. Gao, Z. Liu and C. Duan, *Adv. Energy Mater.*, 2023, **13**, 2204394.
 - 42 P. W. M. Blom, V. D. Mihailetschi, L. J. A. Koster and D. E. Markov, *Adv. Mater.*, 2007, **19**, 1551–1566.
 - 43 W. Liang, L. Chen, Z. Wang, Z. Peng, L. Zhu, C. H. Kwok, H. Yu, W. Xiong, T. Li, Z. Zhang, Y. Wang, Y. Liao, G. Zhang, H. Hu and Y. Chen, *Adv. Energy Mater.*, 2024, **14**, 2303661.
 - 44 H.-F. Zhi, M. Jiang, H. Zhang, Q. An, H.-R. Bai, M. H. Jee, H. Y. Woo, D. Li, X. Huang and J.-L. Wang, *Adv. Funct. Mater.*, 2023, **33**, 2300878.
 - 45 J. Wang, J. Zhu, C. Li, Y. Lin, Y. Yang, Z. Ma and Y. Lu, *Adv. Funct. Mater.*, 2023, **33**, 2304449.
 - 46 H. Tang, J. Ning, K. Wang, H. Liu, X. Lu, S. Tan, M. Huang and B. Zhao, *ACS Appl. Energy Mater.*, 2023, **6**, 4079–4088.
 - 47 D. He, J. Zhou, Y. Zhu, Y. Li, K. Wang, J. Li, J. Zhang, B. Li, Y. Lin, Y. He, C. Wang and F. Zhao, *Adv. Mater.*, 2024, **36**, 2308909.
 - 48 J. Song, L. Ye, C. Liu, Y. Cai, C. Zhang, G. Yue, Y. Li, M. H. Jee, Y. Zhao, D. Wei, H. Y. Woo and Y. Sun, *Energy Environ. Sci.*, 2023, **16**, 5371–5380.
 - 49 H. Xiang, F. Sun, X. Zheng, B. Gao, P. Zhu, T. Cong, Y. Li, X. Wang and R. Yang, *Adv. Sci.*, 2024, **11**, 2401330.